JOURNAL OF GEOPHYSICAL RESEARCH, VOL. 113, D07208, doi:10.1029/2007JD009005, 2008

Click Here for Full Article

Modeling the transport and optical properties of smoke plumes from South American biomass burning

R. I. Matichuk,[1,3,4] P. R. Colarco,[2] J. A. Smith,[1] and O. B. Toon[1]

Received 25 May 2007; revised 16 November 2007; accepted 7 January 2008; published 15 April 2008.

[1] This study investigates the transport and optical properties of smoke plumes from South American biomass burning by using an aerosol transport and microphysical model. In general, the model can reproduce the smoke aerosol optical properties observed by satellite and ground-based instruments during the Large-Scale Biosphere-Atmosphere Experiment in Amazonia - Smoke Aerosols, Clouds, Rainfall and Climate (LBA-SMOCC) campaign. The simulated spatial distribution of smoke aerosol loading over South America also compares well to satellite observations, suggesting that the transport processes in the model are adequate over this region. The results further suggest that the emissions provided by version 2 of the Global Fire Emissions Database are too low over South America. However, wet deposition may be too aggressive in the model. Since the model wet deposition does not include the feedback smoke may have on cloud formation and precipitation suppression, too many aerosols may be removed. Surprisingly, given the different vegetation types, the model simulations also suggest that similar initial particle size distributions and aerosol optical properties can be used to simulate smoke from both African savanna and South American forest fires. However, to reproduce the observed smoke aerosol optical properties over South America, humidification of smoke aerosols needs to be considered. Model results and observations both suggest that the typical single scattering albedo of smoke over South America and Africa differ because of relative humidity, not vegetation type. Overall, this work suggests strategies for improved treatment of South American smoke plumes in climate and microphysical models.

Citation: Matichuk, R. I., P. R. Colarco, J. A. Smith, and O. B. Toon (2008), Modeling the transport and optical properties of smoke plumes from South American biomass burning, *J. Geophys. Res.*, *113*, D07208, doi:10.1029/2007JD009005.

1. Introduction

[2] Investigations in the tropics have shown that biomass burning injects vast amounts of smoke into the atmosphere [*Crutzen and Andreae*, 1990; *Hao et al.*, 1990]. The biomass burning in the tropical region mostly occurs in South America and Africa. In the Amazon Basin, slash-and-burn techniques are widely used for both primary deforestation and seasonal burning of secondary forests and pastures. These biomass burning events produce radiatively effective and chemically active aerosols and trace gases. The light scattering and absorption by these aerosols affects the radiation budget and decreases local and regional visibility. Additionally, smoke aerosols can serve as effective cloud condensation nuclei (CCN) which leads to the modification of cloud properties and lifetimes [*Warner and Twomey*, 1967]. Overall, the magnitude of the global mean radiative forcing due to these aerosols is highly uncertain [*Intergovernmental Panel on Climate Change*, 2001].

[3] This paper focuses on modeling the transport and optical properties of biomass burning aerosols over South America during September 2002. We chose this time frame because it corresponds to the dry season of the Large-Scale Biosphere-Atmosphere Experiment in Amazonia – Smoke Aerosols, Clouds, Rainfall and Climate (LBA-SMOCC) campaign. This field study was devised to study the connection between biomass burning aerosols and cloud microphysics over the Amazon Basin [*Andreae et al.*, 2004].

[4] Climate models seek to properly represent the properties of light absorbing aerosols. For this reason, the goal of this study is to develop a set of measurement-based initial conditions to specify the aerosol emissions, injection altitude, particle size distribution, and optical properties of smoke aerosols in climate models. Comparisons among the model and various surface and satellite-based measurements collected during LBA-SMOCC are made to validate the model's performance. The results from this study should be useful for simulating climate responses from smoke plumes. This work also suggests strategies for improving the treatment of smoke aerosols from South American biomass burning in climate and microphysical models.

[1]Laboratory for Atmospheric and Space Physics, Department of Atmospheric and Oceanic Sciences, University of Colorado, Boulder, Colorado, USA.
[2]NASA Goddard Space Flight Center, Greenbelt, Maryland, USA.
[3]Now at Earth System Research Laboratory, National Oceanic and Atmospheric Administration, Boulder, Colorado, USA.
[4]Also at Cooperative Institute for Research in Environmental Sciences, University of Colorado, Boulder, Colorado, USA.

Copyright 2008 by the American Geophysical Union.
0148-0227/08/2007JD009005$09.00

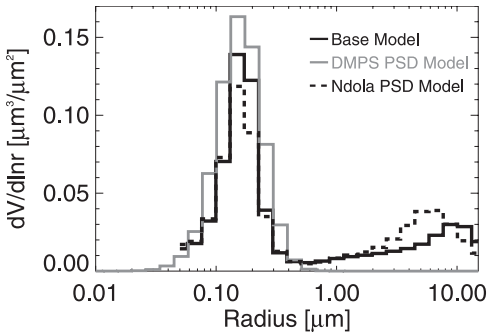

Figure 1. Initial particle size distribution emitted in the base (black line), DMPS PSD (gray model), and African conditions and African PSD (dashed black line) models.

[5] Below, section 2 describes the model and input parameters used to simulate smoke aerosols in the "base" model. Section 3 presents the base model results and compares them to observations made during September 2002. Section 4 presents the results from various sensitivity tests. Section 5 discusses the similarities between African grassland and South American forest smoke simulations. Section 6 discusses the uncertainties in the observations and model. Last, section 7 concludes with a discussion of the current ability to successfully model smoke aerosols produced from biomass burning fires over South America.

2. Model Description

2.1. Aerosol Transport and Dynamical Component

[6] An offline three-dimensional aerosol microphysical and transport model is used in this study. This model is a version of the Community Aerosol and Radiation Model for Atmospheres (CARMA) developed at NASA and the University of Colorado [*Toon et al.*, 1988; *Ackerman et al.*, 1995]. The aerosol transport and removal processes are handled using dynamical and physical fields provided by the National Center for Environmental Prediction (NCEP) reanalysis package (NCEP/NCAR reanalyses [*Kalnay et al.*, 1996]) and the National Center for Atmospheric Research (NCAR) Model for Atmospheric Transport and Chemistry (MATCH) [*Rasch et al.*, 1997].

[7] Using the same temporal and spatial resolution as the NCEP/NCAR reanalyses, CARMA is run from 1 August 2002 to 30 September 2002 on a limited area grid (180°W to 180°E and approximately 15°N to 60°S). In this case, the NCEP/NCAR reanalyses are gridded at T63 horizontal resolution (approximately 1.875° × 1.875°) with 28 vertical sigma layers extending from the surface to approximately 35 km and are available each day at 0000, 0600, 1200, and 1800 UTC. The 6-h meteorological fields generated by the NCEP/NCAR reanalyses and MATCH are linearly interpolated to half-hour timesteps in CARMA.

[8] The microphysical evolution of the particle size distribution in CARMA develops through size specific processes of sedimentation, dry deposition, wet removal, and coagulation. Briefly, the model's advective and diffusive transport processes are calculated using a piecewise parabolic scheme following *Lin and Rood* [1996] and affect each size bin independently. The particle transport by sedimentation is incorporated into the vertical transport and computed for each size bin following *Pruppacher and Klett* [1997]. The wet removal (or "scavenging") follows the treatment by *Barth et al.* [2000] and is uncoupled from the vertical advection equation where it is applied after the transport calculation. Here the aerosols are either affected by cumulus precipitation or stratiform precipitation and evaporation. The coagulation of aerosols in our model increases the mean radius of the particle size distribution at a rate approximately proportional to the air temperature, the square of the particle number concentration, and the inverse of the particle radius [*Pruppacher and Klett*, 1997]. We use a "full solution" algorithm where a single size bin coagulates with the remaining size bins while preserving the total aerosol volume but decreasing the number concentration of particles as small particles stick together and grow larger [*Toon et al.*, 1988]. Although the condensation of gases onto the smoke aerosols may occur, we do not simulate this process in our model. Since this process occurs immediately after the plume leaves the flame zone [*Reid et al.*, 2004a], we cannot resolve this process in our model using such a coarse spatial resolution.

[9] This study also includes the dry deposition calculation tested by *Matichuk et al.* [2007]. Briefly, this parameterization investigated by *Matichuk et al.* [2007] calculates particle dry deposition velocities as a function of particle size and density, vegetation classifications, and relevant meteorological variables. It also includes deposition processes, such as turbulent transfer, Brownian diffusion, impaction, interception, gravitational settling, and particle rebound [*Zhang et al.*, 2001]. These processes, along with the coupling of CARMA to MATCH and the NCEP/NCAR reanalyses, are discussed in more detail in the work of *Colarco et al.* [2002, 2003a, 2003b, 2004] and *Matichuk et al.* [2007].

[10] As suggested by *Matichuk et al.* [2007] to obtain optically accurate results, 22 discrete particle size bins spaced in radius between 0.05 and 15 μm are used to resolve the particle size distribution. This is the same bin separation the Aerosol Robotic Network (AERONET) [*Holben et al.*, 1998; *Dubovik and King*, 2000] uses to report particle size distributions. The initial particle size distribution selected for this study is based on the daily mean AERONET almucantar scans retrieved at Jaru Reserve, Brazil on 20 September 2002 (Figure 1, solid black line). This particular initial particle size distribution is selected because of the site's proximity to the smoke emissions sources and high daily mean AOT at 500 nm (AOT_{500}), suggesting that this site is dominated by locally generated smoke aerosols. In addition to these conditions, this day is selected because it has a low average relative humidity (i.e., relative humidity less than 50%). The relative humidity used here was calculated using the values provided by MATCH and the NCEP/NCAR reanalyses and based on the average between the surface and about 4 km. A day with low relative humidity or a "dry" particle size distribution is most favorable to use as an initial condition since the humidification of the smoke aerosols is treated in the

Table 1. Input Parameters Used in the Base Model

Parameter	Values
Microphysical Processes	advection, coagulation, dry deposition, wet removal, and sedimentation
Emissions Data Set	TPM emissions provided by GFEDv2 [*van der Werf et al.*, 2006]
Emission Rate Over Entire Model Domain	constant throughout month; August: 5.02 Tg; September: 5.82 Tg
Injection Height	mixed between surface and PBLH
Diurnal Cycle	aerosol emitted for 12-h period during daylight hours
Particle Density	1.35 g cm^{-3} [*Reid et al.*, 1998]
Emitted Particle Size Distribution	based on AERONET retrieval at Jaru Reserve on 20 September 2002
Humidification Parameterization	follows *Rissler et al.* [2006], parameters represent conditions during dry period
Refractive Index	$N_{ref} = 1.50 - 0.02i$ (applied at all wavelengths)

optical property calculations (see section 2.3). Additionally, each bin is assumed to be internally mixed so that all the particles within a bin are assumed to have the same chemical composition. The input parameters used in the "base" model are summarized in Table 1.

2.2. Smoke Source Component

[11] The smoke emissions are interpolated from the latest version of the Global Fire Emissions Database (GFEDv2), which provides a global $1° \times 1°$ gridded monthly mean map of various aerosols and trace gas species [*van der Werf et al.*, 2006]. The emissions are interpolated to the model grid by performing an area weighted spatial averaging from the $1° \times 1°$ gridded map provided by GFEDv2 to the CARMA grid. This version of GFED uses a biogeochemical model that has been modified to account for fires [*van der Werf et al.*, 2003], in combination with a burned area time series derived from the Moderate Resolution Imaging Spectroradiometer (MODIS) satellite sensors [*Giglio et al.*, 2006]. Although significant efforts have been made to improve global biomass burning estimates, uncertainties are still large and difficult to quantify [*van der Werf et al.*, 2006].

[12] The total particulate matter (TPM) emissions provided by GFEDv2 are used in this study. These emissions use emission factors provided by *Andreae and Merlet* [2001] and the assumption that 45% of the dry mass burned is carbon. On the basis of the results found by *Matichuk et al.* [2007], the fires are assumed to emit aerosols at a constant rate each day. *Matichuk et al.* [2007] also conducted various sensitivity tests to investigate a proper method for emitting smoke aerosols into the simulated atmosphere over southern Africa. The results from *Matichuk et al.* [2007] found that the simulated aerosol fields most closely matched the observations when the smoke was distributed within the boundary layer. Therefore as suggested by *Matichuk et al.* [2007], the smoke is distributed between the surface layer of the model and the layer associated with the top of the planetary boundary layer (PBL) reported by MATCH. On average, the MATCH planetary boundary layer height (PBLH) at the selected study sites peaked in the afternoon with heights between 0.5 and 2.0 km. A study by *Prins et al.* [1998] showed an evident diurnal signature in fire activity throughout the burning season of the Smoke, Clouds, and Radiation in Brazil (SCAR-B) experiment in 1995. Using fire count information retrieved by the Geostationary Operational Environmental Satellite (GEOS-8), the peak burning over Brazil was observed to occur in the early to midafternoon local time [*Prins et al.*, 1998]. For this reason, the smoke emissions in the base case are concentrated during a 12-h period starting in the morning to represent a diurnal cycle in the model. Over the model domain, which includes most of the Southern Hemisphere (globally between 15°N to 60°S), the total smoke emissions are about 5.02 Tg in August and 5.82 Tg in September, where 1.85 Tg and 1.23 Tg of the total emissions are produced over South America in August and September, respectively. The remaining emissions mainly occur over southern Africa. Figure 2 shows the spatial distribution of smoke emissions interpolated to the model grid over South America for September 2002. Note that this study only includes aerosol sources of chemically

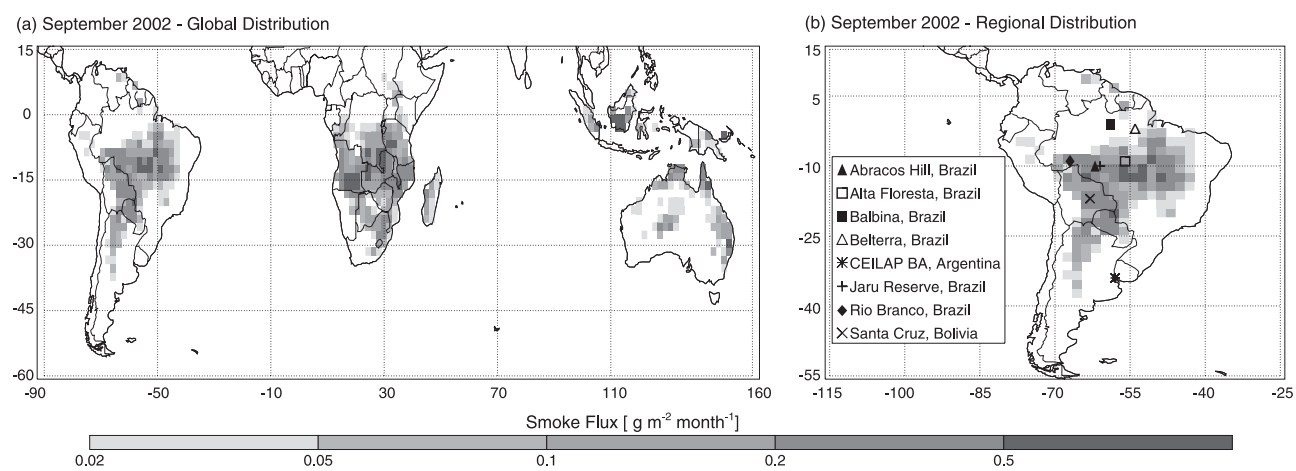

Figure 2. Spatial distribution of monthly mean smoke emissions interpolated from the GFEDv2 data set over South America during September 2002. (a) The global distribution of the smoke emissions over the model domain. (b) The regional distribution of the smoke emissions over South America. Also shown are the AERONET sites used for model validation.

inert smoke particles generated from biomass burning. Other sources, such as dust, sea salt, and anthropogenic and biogenic aerosols, that may exist in this region are not included in this study.

2.3. Smoke Optical Property Calculations

[13] The aerosol optical thickness (AOT), Ångström parameter (α), single scattering albedo (SSA), and vertical extinction profiles are investigated in this study. The simulated smoke aerosol optical properties are calculated assuming Mie scattering [*Wiscombe*, 1979] of homogeneous aerosols with a density of 1.35 g cm^{-3} [*Reid et al.*, 1998]. Since AERONET only retrieves the aggregate of all aerosol properties, the aerosols in the model are not partitioned into different aerosol species. Here, the aerosols are treated as internal mixtures of organic carbon (OC) and black carbon (BC), with size and optical properties constrained by AERONET observations. A wavelength-independent refractive index ($N_{ref} = 1.50-0.02i$) that represents the daily mean refractive index at 440 nm as retrieved by AERONET at Jaru Reserve, Brazil on the same day as the selected initial particle size distribution (20 September 2002) is used in the optical property calculations. A volume weighting approach is also used to mix the refractive index of smoke aerosols with the refractive index of water (1.33–0.00*i*) to adjust for relative humidity.

[14] The humidification of the smoke aerosols is treated in the optical property calculations following a parameterization described by *Rissler et al.* [2006]. *Rissler et al.* [2006] measured the hygroscopic properties of fine mode smoke aerosols using a Hygroscopic Tandem Differential Mobility Analyzer (H–TDMA) over the southwestern region of the Amazon during the LBA–SMOCC campaign. This study found that the relative humidity scans did not display any obvious step-like deliquescent behavior; instead, all scans were found to be fitted with a continuous one-parameter function. Therefore, the growth factor formula provided by *Rissler et al.* [2006, equations (2) and (3)] and the midday, dry period average parameters are used to age the simulated smoke aerosols over South America. Since this parameterization represents fine mode particles, this formula is applied to particles with radii smaller than 2.0 μm. The impacts of this humidification parameterization are discussed in section 4.

[15] Similar to *Matichuk et al.* [2007], the monthly mean optical property calculations only include days dominated by smoke aerosols. Accordingly, the day is classified as being "smoke-dominated" when the daily average AOT_{500} retrieved by AERONET is greater than 0.30. The same aggregation and sampling strategy developed by *Matichuk et al.* [2007] is used to provide a means for the satellite retrievals to be compared to the model results. This method aggregates the highest quality pixels from the Level 2 satellite products to the model grid, and then the average retrieved AOT_{550} is calculated based on pixel thresholds. The pixel threshold is a function of the satellite instrument. A certain number of observations are required for each satellite to fall within the model grid box on a particular day for that day to count in the monthly average. This number is 15 and 5 for MODIS and MISR, respectively. This threshold is somewhat arbitrary, but the threshold chosen is such that the result is not very sensitive to small variations about this threshold. It is meant to allow additional constraint so that cloud contaminated retrievals do not adversely affect the result. Since satellites do not frequently overlap in time at a single location, there is a unique model average AOT_{550} for each satellite where the simulated monthly mean only includes the times and locations at which the satellite made retrievals. This allows the satellite retrievals to be directly compared to the simulated AOT_{550} at the model resolution.

3. Discussion of Model Results

[16] In this section, the simulated optical properties from the model are compared to ground and satellite-based measurements made over South America during September 2002. This section also provides a discussion of how well the initial input parameters represent the distributions of smoke aerosols near the smoke source regions. The model results are compared to observations at eight sites: Abracos Hill, Alta Floresta, Balbina, Belterra, Jaru Reserve, and Rio Branco in Brazil; CEILAP BA in Argentina; and Santa Cruz, Bolivia (Figure 2). These sites are used for model validation because of the amount of available data collected and their proximity to the smoke source regions. The simulated optical properties are compared to retrievals made by AERONET [*Holben et al.*, 1998], the Micro-Pulse Lidar Network (MPLNET) [*Spinhirne et al.*, 1995], MODIS [*Kaufman et al.*, 1997; *Tanré et al.*, 1997], and MISR [*Diner et al.*, 1998; *Martonchik et al.*, 1998].

3.1. Comparisons of Monthly Mean Aerosol Optical Thickness to Satellite and Ground-Based Observations

[17] Table 2 presents the monthly mean AOT_{500} of smoke-dominated days retrieved by AERONET and simulated by the base model at selected study sites during September 2002. The top four sites with the largest number of smoke-dominated days are presented in Table 2. In this study, level 2.0 cloud-screened, quality-assured AERONET data [*Smirnov et al.*, 2000] are used to compare to the model results. In this comparison, the monthly mean AOT_{500} simulated by the base model is approximately 90% lower than AERONET. Table 3 presents the mean AOT_{550} of smoke-dominated days simulated by the base model and retrieved by MODIS and MISR at the same AERONET sites selected for Table 2 during September 2002. The mean includes days when both satellite instruments made retrievals at the selected locations, and the data was aggregated to the model resolution before the average was computed, which explains the low number of days included in the mean. In this comparison, the simulated mean AOT_{550} of the base model is about 85% lower than the retrievals.

[18] Assuming that all of the aerosols were derived from biomass burning sources, the smoke source function needs to be scaled up by a factor of about six for the model to reproduce the AOT observed by the satellites and AERONET. This model will be referred to as the "scaled model." In comparisons between AERONET AOT_{500} retrievals and results from the scaled model, there is about a 10% difference between AERONET and the model at the selected study sites (see Figure 3 and "scaled" model in Table 2). In comparisons between the satellite AOT_{550} retrievals and the scaled model, there is about a 15% difference between the satellite retrievals and model (see

Table 2. Monthly Mean Retrieved and Simulated Optical Properties of Smoke-Dominated Days at Selected Study Sites Over South America During September 2002[a]

	Abracos Hill, Brazil			Alta Floresta, Brazil			Jaru Reserve, Brazil			Rio Branco, Brazil		
	AOT_{500}	$\alpha_{440/870}$	SSA_{440}	AOT_{500}	$\alpha_{440/870}$	SSA_{440}	AOT_{500}	$\alpha_{440/870}$	SSA_{440}	AOT_{500}	$\alpha_{440/870}$	SSA_{440}
Number of days in mean	20	20	7	16	16	6	27	27	10	20	20	8
AERONET OBS.	1.15 (0.62)	1.87 (0.13)	0.96 (0.013)	1.42 (0.68)	1.72 (0.24)	0.97 (0.014)	1.05 (0.73)	1.79 (0.21)	0.94 (0.015)	0.74 (0.51)	1.75 (0.26)	0.94 (0.011)
Base	0.18 (0.088)	1.78 (0.20)	0.97 (0.011)	0.19 (0.086)	1.83 (0.18)	0.97 (0.013)	0.12 (0.064)	1.82 (0.17)	0.96 (0.012)	0.13 (0.074)	1.75 (0.20)	0.97 (0.013)
Scaled	1.18 (0.60)	1.61 (0.21)	0.97 (0.011)	1.26 (0.59)	1.67 (0.18)	0.97 (0.011)	0.81 (0.43)	1.66 (0.17)	0.96 (0.011)	0.81 (0.49)	1.57 (0.19)	0.97 (0.012)
Daily emissions	1.28 (0.76)	1.62 (0.21)	0.97 (0.011)	1.92 (0.64)	1.65 (0.22)	0.97 (0.013)	0.84 (0.41)	1.64 (0.20)	0.96 (0.011)	0.74 (0.39)	1.55 (0.24)	0.97 (0.011)
Weekly emissions	1.14 (0.48)	1.63 (0.22)	0.97 (0.011)	1.41 (0.78)	1.68 (0.20)	0.97 (0.012)	0.78 (0.36)	1.67 (0.17)	0.96 (0.011)	0.76 (0.42)	1.59 (0.20)	0.97 (0.012)
No hygros. Growth	0.97 (0.59)	1.79 (0.088)	0.90 (0.0013)	1.17 (0.58)	1.79 (0.065)	0.90 (0.001)	0.71 (0.40)	1.79 (0.072)	0.90 (0.001)	0.64 (0.42)	1.79 (0.072)	0.90 (0.001)
No wet removal	1.82 (0.84)	1.45 (0.21)	0.97 (0.012)	1.82 (0.92)	1.54 (0.22)	0.97 (0.012)	1.40 (0.71)	1.49 (0.18)	0.96 (0.012)	1.52 (0.89)	1.38 (0.21)	0.97 (0.012)
Feedback 1	1.29 (0.62)	1.59 (0.21)	0.97 (0.011)	1.36 (0.67)	1.65 (0.19)	0.97 (0.012)	0.90 (0.48)	1.63 (0.17)	0.96 (0.012)	0.93 (0.57)	1.54 (0.20)	0.97 (0.012)
Feedback 2	1.47 (0.72)	1.54 (0.21)	0.97 (0.012)	1.52 (0.79)	1.61 (0.21)	0.97 (0.012)	1.04 (0.56)	1.59 (0.17)	0.96 (0.012)	1.08 (0.66)	1.49 (0.20)	0.97 (0.012)
African conditions	1.03 (0.53)	1.59 (0.19)	0.96 (0.014)	1.11 (0.52)	1.65 (0.17)	0.96 (0.014)	0.71 (0.38)	1.63 (0.15)	0.95 (0.014)	0.71 (0.43)	1.55 (0.18)	0.96 (0.015)
African PSD	1.03 (0.52)	1.60 (0.19)	0.97 (0.012)	1.10 (0.51)	1.65 (0.17)	0.97 (0.013)	0.71 (0.38)	1.64 (0.15)	0.96 (0.012)	0.71 (0.43)	1.56 (0.18)	0.96 (0.013)

[a]The numbers listed in parentheses represent the standard deviations.

Table 3. Mean AOT_{550} of Smoke-Dominated Days Retrieved by MODIS, MISR, and Simulated by Various Models at Selected Study Sites and on the Same Days During September 2002[a]

	Abracos Hill, Brazil	Alta Floresta, Brazil	Jaru Reserve, Brazil	Rio Branco, Brazil
Number of days in mean	3	4	4	6
MODIS retrieval	1.16 (0.68)	0.98 (0.38)	0.66 (0.21)	0.41 (0.23)
MISR retrieval	0.81 (0.32)	0.80 (0.22)	0.50 (0.17)	0.38 (0.25)
Base model	0.11 (0.069)	0.14 (0.083)	0.10 (0.078)	0.04 (0.080)
Scaled model	0.84 (0.48)	0.93 (0.56)	0.64 (0.35)	0.48 (0.27)

[a]The numbers listed in parentheses represent the standard deviations.

Figure 4 and "scaled" model in Table 3). Similar to the results from *Matichuk et al.* [2007] over southern Africa, there is a discrepancy between the MODIS and MISR retrievals. Over continental South America, the monthly mean AOT_{550} retrieved by MISR is about 25% lower than MODIS (Figure 5). The discrepancy observed in the comparison between MODIS and MISR most likely reflects the differences in the retrieval techniques and does limit the ability to use the satellite data to assess the performance of the model. However, the model results are correlated with the satellite observations, suggesting that the differences represent systematic errors, rather than random errors.

[19] Similar to the results from *Matichuk et al.* [2007] over southern Africa, the results from this study also show a linear relationship between the mass of smoke emitted in the model and simulated AOT over South America. However, in the work of *Matichuk et al.* [2007], the smoke emissions, which were interpolated from GFEDv1, needed to be scaled up by about 30% for an optimum fit. Owing to the uncertainties in the smoke source function, which will be discussed in more detail below, and for the initial convenience in validating the model's performance, the model which scales the smoke source function up by a factor of six (i.e., scaled model) will be used throughout the rest of the paper.

[20] During the last week of September 2002, MODIS observed a large-scale biomass burning event over Brazil (see http://eospso.gsfc.nasa.gov/eos_observ/pdf/May-

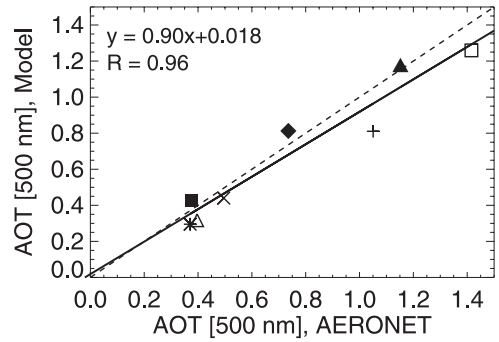

Figure 3. Scatterplot of monthly mean AOT_{500} of smoke-dominated days simulated by scaled model versus AERONET at selected study sites during September 2002. The dashed line represents the 1-to-1 line and the solid line represents the line of best fit. Each site is represented by a different symbol: Abracos Hill (solid triangle); Alta Floresta (open square); Balbina (solid square); Belterra (open triangle); CEILAP BA (star); Jaru Reserve (plus symbol); Rio Branco (solid diamond); Santa Cruz (cross symbol).

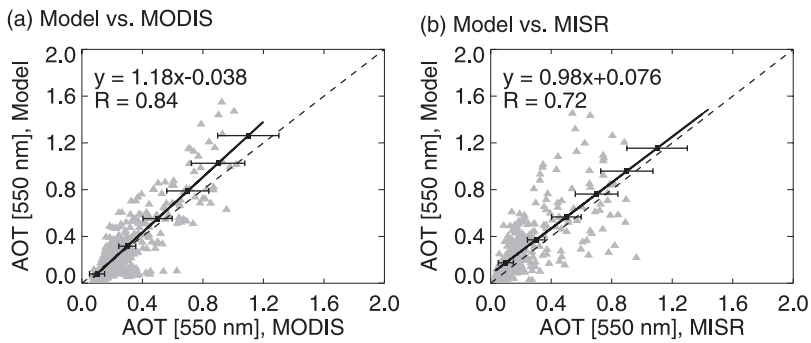

Figure 4. Scatterplots of monthly mean AOT_{550} simulated by the scaled model versus observations over South America during September 2002. The dashed line represents the 1-to-1 line and the solid line represents the line of best fit. For clarity, the uncertainty in the satellite retrievals is grouped into intervals of 0.20. The error bars in these figures represent the mean uncertainty in the satellite data at each interval.

Jun06.pdf). To determine if the model has the correct spatial distribution of the smoke plumes during this burning event (i.e., 20–30 September 2002), the mean AOT_{550} simulated by the scaled model is compared to MODIS and MISR (Figure 6). The model produces a similar spatial distribution in AOT_{550} as the satellite observations with the greatest aerosol loading over central South America (i.e., roughly between 8°S and 25°S and 45°W and 70°W). Qualitatively, this simple comparison shows that the simulated smoke plumes are in roughly the same locations as measured by the satellites and demonstrates the model's ability to transport smoke aerosols properly over a large region. A quantitative comparison of the model results and observations during this time period will be investigated in section 4.

[21] Overall, these results suggest that the carbon emissions provided by GFEDv2 and/or the assumed emission factors used to convert the carbon emissions into TPM are too low. Since the burned area estimates and fire counts in these regions are poorly constrained, the carbon emissions provided by GFEDv2 are highly uncertain. Alone, the burned area product provided by MODIS has an uncertainty of about 50%. In addition, the emissions from tropical regions undergoing deforestation are known to be low and are particularly difficult to quantify because of the consistent cloud cover and the large spatial heterogeneity that exists in these regions [*van der Werf et al.*, 2006]. Comparisons against measurements of atmospheric CO prove especially useful since biomass burning is a major source of CO [*van der Werf et al.*, 2003]. According to G. van der Werf (personal communication, 2006) and inverse modeling studies by G. Pétron et al. (manuscript in preparation, 2008), carbon monoxide (CO) emissions provided by GFEDv2 are up to a factor of two lower than the Measurement Of the Pollution In The Troposphere (MOPITT) observations [*Deeter et al.*, 2003] over South America. In addition to the uncertainty in the carbon burned provided by GFEDv2, the emission factors used to generate the GFEDv2 TPM emissions may also produce errors in the simulated AOT. The emission factors applied in GFEDv2 are provided by *Andreae and Merlet* [2001] and have uncertainties of about 40%. Another factor that may contribute or produce errors in the simulated AOT may be the contribution of other aerosol species, such as sea salt and anthropogenic and biogenic emissions, which are not considered in this study. Additionally, incorrect parameterization of washout of smoke aerosols may generate errors in the simulated optical properties. This issue is discussed in more detail in section 4.4.

3.2. Comparisons of Monthly Mean Spectral Dependences of the Aerosol Optical Thickness and Single Scattering Albedo to AERONET Retrievals

[22] In this section, the monthly mean spectral dependence of AOT for smoke-dominated days simulated by the scaled model is compared to AERONET data at selected study sites. Figure 7 shows the spectral dependence of the AOT simulated by the scaled model and retrieved by AERONET at six sites in South America. The magnitude of the simulated AOT compares well to AERONET, and the maximum difference between the model and AERONET is about 30% (see Table 2).

[23] Figure 8 shows the spectral dependence of SSA at four sites in South America. In general, the aerosols simulated in the scale model are slightly less absorbing than AERONET. However, the simulated SSA are within the accuracy (±0.03) of the AERONET retrievals [*Eck et al.*, 1999]. In comparisons among the base and scaled models, the magnitude of the simulated SSA is not sensitive to the

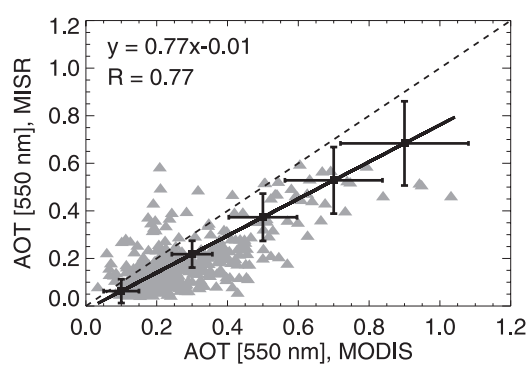

Figure 5. Scatterplots of monthly mean AOT_{550} retrieved by MODIS versus MISR over South America during September 2002. The dashed line represents the 1-to-1 line and the solid line represents the line of best fit. For clarity, the uncertainty in the satellite retrievals is grouped into intervals of 0.20. The error bars in these figures represent the mean uncertainty in the satellite data at each interval.

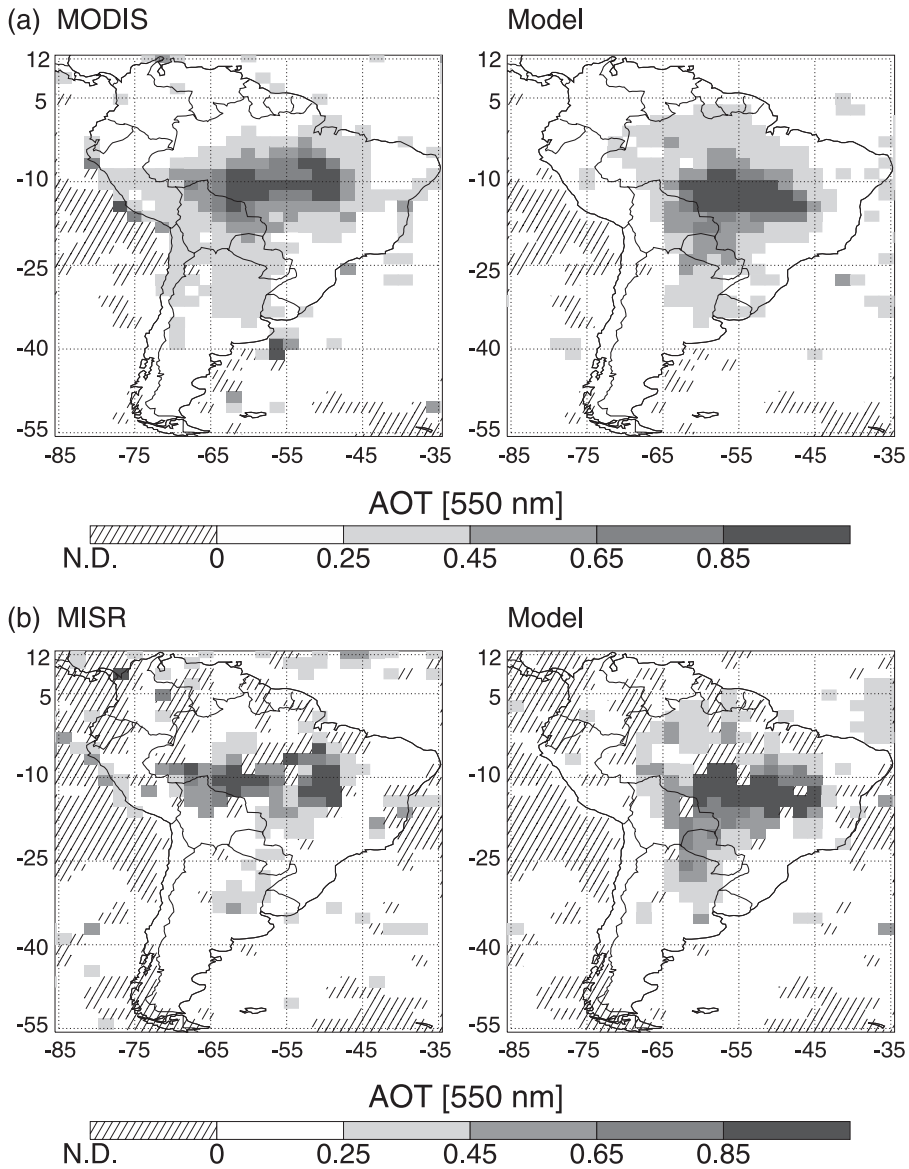

Figure 6. Mean AOT_{550} between September 20th and September 30th of 2002 over South America. (a) Comparisons between MODIS and Scaled model. (b) Comparisons between MISR and Scaled model. The hatch marks represent grid boxes with no data (N. D.). Note that the model results shown in Figures 6a and 6b are from the same simulation. The differences in the figures reflect how the model results are sampled differently for comparison to the satellite results (see section 2.3).

emitted smoke mass (see Table 2). These results are expected since SSA is not a mass-dependent property but instead is dependent on the fraction of light scattered as it interacts with the particles.

[24] Since the scattering due to particles is much larger than the absorption, the spectral dependence of AOT can be used to understand the size of the particles. In most cases, as a measurement becomes dominated by larger particles, the AOT will become wavelength independent (i.e., slope of spectral dependence will flatten). The AOT retrieved by AERONET and simulated by the scaled model is found to decrease with increasing wavelength (see Figure 7), indicating that the particles are small compared with the wavelength. The fact that a wavelength independent refractive index can be used to reproduce the observed spectral dependence was previously noted by *Bergstrom et al.* [2002] and *Matichuk et al.* [2007] for smoke from savanna fires in southern Africa.

[25] A variable commonly used to quantify the spectral dependence of AOT and the sizes of the particles is the Ångström parameter (α). Typical values of α range from around 2.0 for fresh smoke particles that are dominated by accumulation mode aerosols to nearly zero for coarse mode aerosols [*Eck et al.*, 1999]. Figure 9 shows the monthly mean Ångström parameter of smoke-dominated days retrieved by AERONET and simulated by the scaled model. In general, the model compares fairly well to the AERONET data at the selected study sites. At all study sites, except Belterra, the model is simulating particles that have slightly lower Ångström parameters than observed by AERONET. At Belterra, the simulated Ångström parameter is higher than AERONET observations suggesting that the

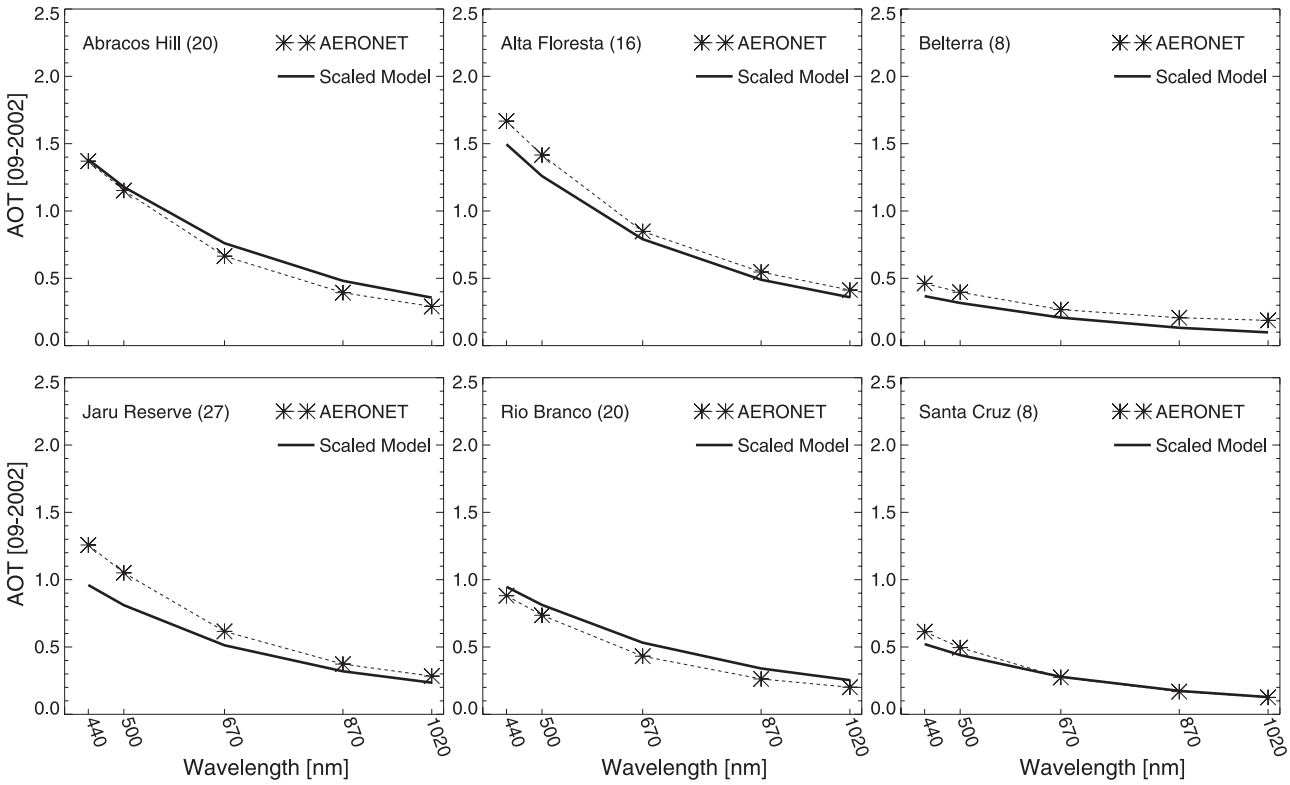

Figure 7. Monthly mean spectral dependence of AOT retrieved by AERONET and simulated by scaled model during September 2002. The monthly mean only includes smoke-dominated days. The number of smoke-dominated days is listed in parentheses.

model has more smaller-sized particles. Since Belterra is near the Atlantic Ocean, this site may be impacted by sea salt aerosols. Therefore, the lower Ångström parameter observed by AERONET at Belterra may be a result of these large sea salt aerosols. Given that the model is not simulating sea salt aerosols, the Ångström parameter is expected to be higher than the AERONET data. Additionally, the humidification parameterization may not be appropriate at this location. Even though CEILAP BA is located near the coast, the Ångström parameter simulated by the model compares well to the AERONET retrievals. This result may be due to the meteorological conditions at this site. According to the NCEP reanalyses during September 2002, the winds generally flow from the west at CEILAP BA. Therefore, the westerly winds would prevent CEILAP BA from being significantly impacted by coarse-sized sea salt aerosols. It is remarkable that the same initial emitted particle size distribution can be used at most of the study sites to reproduce the observed Ångström parameter given that the vegetation burned is different. Comparisons among the base and scaled models also show that the Ångström parameter is slightly sensitive to the emitted smoke mass. The simulated Ångström parameter decreases by about 10% or less when the smoke mass is increased by a factor of six (see Table 2). The changes in the simulated Ångström parameter are most likely due to coagulation. By increasing the amount of smoke mass, the rate of coagulation is increased, thereby increasing the median radius of the particles.

[26] According to *Bergstrom et al.* [2002], since the SSA is the ratio of the scattering from aerosols to total extinction, the wavelength dependence of SSA depends on whether the absorption coefficient falls off faster or slower with wavelength than the scattering coefficient. In general, when a measurement is dominated with black carbon (BC), the absorption coefficient falls off slower with wavelength (i.e., about lambda^{-1}) than the scattering coefficient [*Bergstrom et al.*, 2002]. Since the AERONET retrievals and simulated SSA decrease with increasing wavelength (see Figure 8), the absorption coefficient falls off more slowly with wavelength than the scattering coefficient suggesting that BC is dominating the absorption.

3.3. Comparisons of Vertical Extinction Profiles to Lidar Measurements

[27] Figure 10 shows the mean extinction profile at 523 nm simulated by the scaled model and retrieved by the Micro-Pulse Lidar (MPLNET) [*Spinhirne et al.*, 1995] at Abracos Hill, Brazil. The computed mean includes all days when MPLNET was operational during the day (i.e., 12–13 and 15–20 September 2002), and the model is sampled on the same days and near the same time as the measurements. In general, the model generates a similar vertical distribution as the MPLNET measurements suggesting that the vertical transport and vertical distribution of the smoke in the model are adequate at this study location. In particular, both the model and MPLNET retrievals observe a smoke layer below 2 km. However, the simulated extinction at altitudes greater than 2 km is slightly larger than the MPLNET retrievals. These results suggest that too much smoke is being transported into the free troposphere by the model.

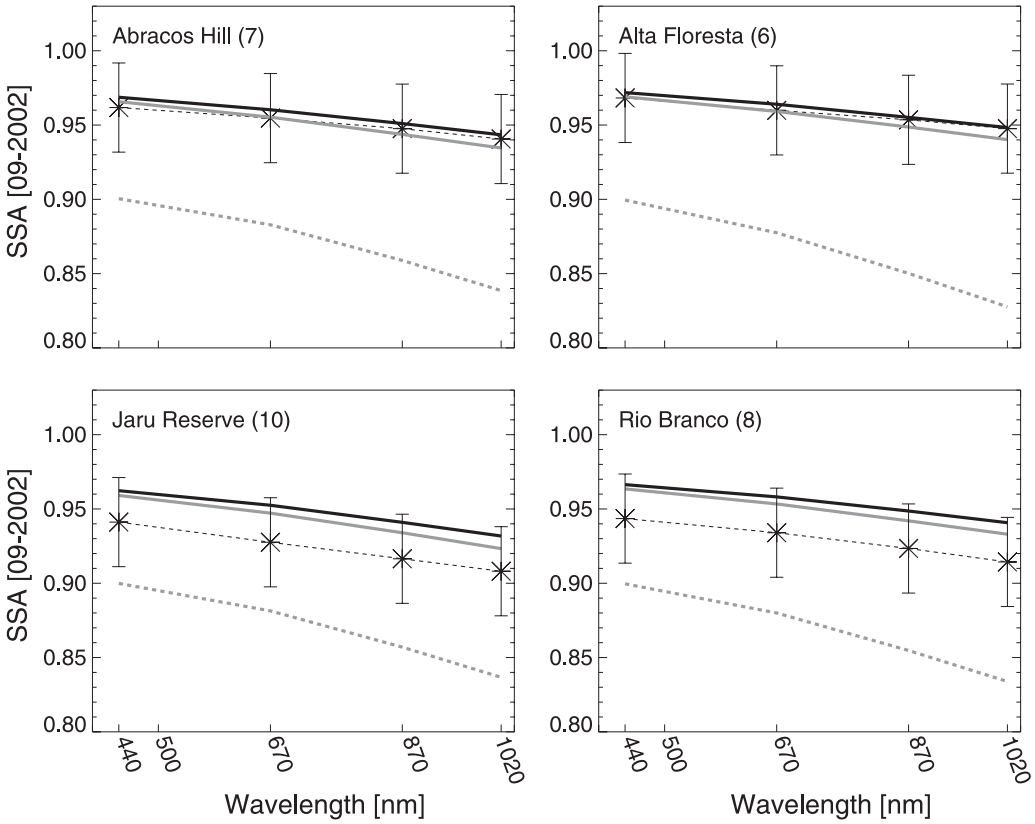

Figure 8. Monthly mean spectral dependence of SSA retrieved by AERONET and simulated by various models during September 2002. The scaled model is represented by the black solid line, African PSD model is represented by the gray solid line, and no hygroscopic growth model is represented by the gray dashed line. The asterisks connected by the black dashed line represent the AERONET retrievals. The monthly mean only includes smoke-dominated days. The number of smoke-dominated days is listed in parentheses.

[28] It has been shown for biomass burning that plume rise can be significant for individual events [e.g., *Westphal and Toon*, 1991; *Lavoué et al.*, 2000; *Colarco et al.*, 2004]; however, observations of biomass burning showed little evidence for plume rise to occur on a regular basis over South America during this time frame. In addition to the MPLNET profiles, vertical profiles of light scattering coefficients at 550 nm from airborne observations also show that on average most of the optically active aerosols were below 2 km during LBA–SMOCC over the Amazon Basin [*Chand et al.*, 2006]. Vertical total attenuated backscattering profiles at 532 nm retrieved by the Cloud-Aerosol Lidar and Infrared Pathfinder Satellite Observations (CALIPSO) instrument [*Winker et al.*, 2002] during September 2006 also show that the aerosols are mixed within the PBL over South America. Since there is little information to constrain the vertical distribution of smoke over South America during this time frame, it is difficult to understand the model deficiencies without more measurements. Therefore, the investigation of plume rise algorithms is a subject of future research.

3.4. Comparisons of Monthly Mean Particle Size Distributions to AERONET Retrievals

[29] Figure 11 presents the monthly mean column-integrated volume particle size distribution on smoke-dominat-

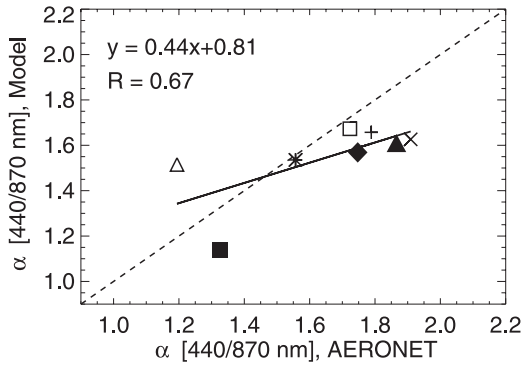

Figure 9. Monthly mean Ångström parameter (440/870 nm) of smoke-dominated days simulated by the scaled model and retrieved by AERONET at selected study sites during September 2002. The dashed line represents the 1-to-1 line and the solid line represents the line of best fit. Each AERONET site is represented by a different symbol: Abracos Hill (solid triangle); Alta Floresta (open square); Balbina (solid square); Belterra (open triangle); CEILAP BA (star); Jaru Reserve (plus symbol); Rio Branco (solid diamond); Santa Cruz (cross symbol).

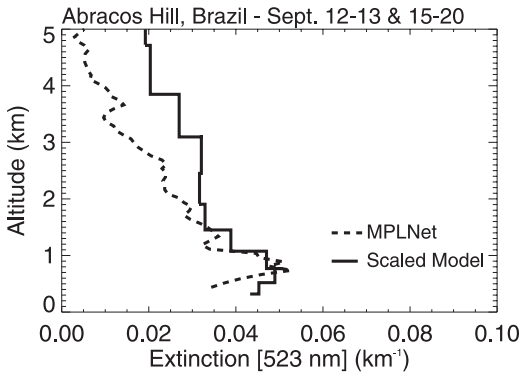

Figure 10. Mean vertical extinction profiles at Abracos Hill, Brazil during September 2002. The scaled model is represented by the black solid line, while the MPLNET retrieval is represented by the black dashed line. Note that the model is sampled during the day near the same time as the measurement.

ed days simulated by the scaled model and retrieved by AERONET at Jaru Reserve, Brazil during September 2002. Compared to the initial emitted particle size distribution (see gray solid line), the peak of the accumulation mode volume distribution of the scaled model has shifted from approximately 0.16 to 0.20 μm. This shift is due to coagulation and humidification of the particles. Compared to the mean AERONET retrievals, the peak of the accumulation mode distribution of the scaled model is similar; however, the simulated accumulation mode distribution contains more particles at radius sizes between 0.3 and 0.7 μm. The comparison of monthly mean Ångström parameter of smoke-dominated days at Jaru Reserve suggests that the simulated median radius is slightly larger than the AERONET retrievals (Table 2). The monthly mean volume median radius of the accumulation mode is 0.17 and 0.22 μm for AERONET and Scaled model, respectively, on smoke-dominated days at Jaru Reserve.

[30] Similar to the results by *Matichuk et al.* [2007], the model may be removing too many coarse mode size particles. It is difficult to determine the model's performance without modeling the other coarse-size particles that may exist at this location and acquiring more information from the scientific community on the composition of these coarse-sized particles. If the coarse mode is composed of ash particles, the density would be lower than the density currently being assumed and the particles could have irregular shapes. As shown by *Matichuk et al.* [2007], assuming different particle shapes and/or densities of the coarse mode particles would improve the comparisons among the model and observations. The investigation of the removal of coarse-mode particles is a subject of future research.

4. Discussion of Results From Sensitivity Tests

[31] A series of tests are conducted to understand the model's sensitivity to various input parameters. These tests explore the model's sensitivity to the smoke source function (section 4.1), initial particle size distribution (section 4.2), relative humidity (section 4.3), and wet removal (section 4.4). Each test is assigned a name, and a summary of the names and variances in each test are presented in Tables 4a and 4b.

4.1. Sensitivity to the Timing of the Smoke Aerosol Emissions

[32] The model's sensitivity to emissions data sets with different temporal resolutions is investigated in this section. There are two additional emissions data sets tested in the model. One data set provides weekly average emissions and is constructed by resampling the monthly mean fire carbon consumption provided by GFEDv2 to an 8-d timestep using MODIS fire hot spots [*Giglio et al.*, 2003a, 2003b]. This model test is referred to as the "weekly emissions" model. The other data set provides daily emissions. This data set uses an aggregation of the MODIS Terra and MODIS Aqua fire hotspot products, which have been calibrated against the GFEDv2 database (A. da Silva, personal communication, 2007). Over the 2-year overlap period of both GFEDv2 and MODIS sensors (i.e., 2003 to 2004), the emissions per fire count are found at each grid box. Here, the 2-year integral of these daily emissions over that period maintains the GFEDv2 emissions, but over a shorter interval of time these derived emissions will not be identical to GFEDv2. However, the monthly spatial patterns are very similar. This method was then extended back to September 2002, which is the earliest availability of both MODIS Terra and Aqua data. Note that no attempt is made to correct for cloud-obscured fires, which may not be detected by the satellite. This will introduce biases where the emissions may be low on a particularly cloudy day and high on a cloud-free day, but in the average the biases reduce to the GFEDv2 database. This model test is referred to as the "daily emissions" model. Since GFEDv2 is found to be too low in this study and both the "weekly" and "daily" emissions data sets originate from GFEDv2, the smoke source functions provided by these data sets are also scaled up by a factor of six.

[33] Figure 12 presents the daily mean AOT_{500} retrieved by AERONET and simulated by the models at Abracos Hill, Brazil to determine, qualitatively, the model's ability to simulate the observed day-to-day fluctuations in AOT_{500} during September 2002. When this site is examined and

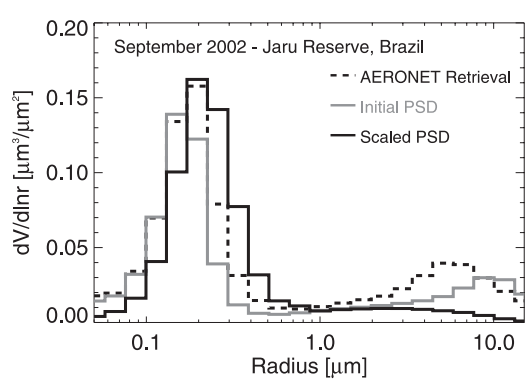

Figure 11. Monthly mean column-integrated volume size distribution retrieved by AERONET (black dashed line) and simulated by the scaled model (black solid line) at Jaru Reserve during September 2002. The mean represents the days dominated by smoke. The gray solid line represents the initial particle size distribution emitted in the model.

Table 4a. Sensitivity Test Names and Modifications Made Relative to the Base Model

Model Name	Parameter Changed in Base Model	New Parameter Description
Scaled model	emission rate	GFEDv2 emissions scaled up by 6
Daily emissions	emission rate	daily emissions data set scaled up by 6
Weekly emissions	emission rate	GFEDv2 8-d emissions data set scaled up by 6
DMPS PSD	size distribution	source function scaled up by six; see Table 4b for particle size distribution properties.
No hygroscopic growth	relative humidity	relative humidity assumed to be zero; source function scaled up by six
No wet removal	microphysical process	no wet removal in model and source function scaled up by six.
Feedback 1	microphysical process	Apply *Koren et al.* [2004] cloud fraction versus AOT function to wet removal routine. Cloud fraction is modified in convective scavenging calculations.
Feedback 2	microphysical process	Apply *Koren et al.* [2004] cloud fraction versus AOT function to wet removal routine. Cloud fraction is modified in convective scavenging calculations and calculations of stratiform scavenging in boundary layer
African conditions	size distribution refractive index	uses particle size distribution and refractive index retrieved by AERONET at Ndola, Zambia during September 2000. The particle size distribution was retrieved on 16 September 2000 and the refractive index represents the monthly mean indices during September 2000 [$N_{ref} = 1.51 - 0.024i$] [see *Matichuk et al.*, 2007]. Source function based on GFEDv2 and scaled up by six.
African PSD	size distribution	uses the particle size distribution retrieved by AERONET at Ndola, Zambia on 16 September 2000. Source function based on GFEDv2 and scaled up by six.

compared to days when AERONET's AOT_{500} peaks, the scaled model's peak AOT_{500} is a day late on 16 and 18 September but is consistent with AERONET on 21 September 2002. Note that the scaled model uses a constant emission rate throughout the month. As shown above in Figure 6, MODIS observed a large biomass burning event that encompassed this site between 20 and 30 September 2002. During this time frame, AERONET also observed this large-scale biomass burning event at Abracos Hill, retrieving AOT_{500} much greater than 1.0 between 20 and 25 of September 2002. In comparisons of the scaled model to AERONET during this time period, the magnitude of simulated daily mean AOT_{500} is much lower. When emissions data sets with finer temporal resolutions (i.e., Figure 12: weekly (gray solid line) and daily emissions (black solid line)) are used in the model, the magnitude of the simulated daily mean AOT_{500} does improve during this burning event, suggesting that the daily emissions data sets are capturing the smoke plumes but the magnitude of the emissions during this particular smoke event are still too low seeing that the simulated AOT_{500} is still much lower than the AERONET retrievals. Quantitatively, Figure 13 shows scatterplots of the daily mean AOT_{500} retrieved by AERONET and simulated by the three models. Even though the monthly mean AOT simulated by the scaled model compares well to AERONET (R = 0.96; see Figure 3), on a daily basis there is a poor correlation between the model and AERONET. In the comparisons among the three models and AERONET, both the line of best fit and correlation coefficient improves when the temporal resolution of the smoke emissions data set increases (Figure 13).

[34] Similar to the results found by *Myhre et al.* [2003] and *Matichuk et al.* [2007], these model results suggest that the transport processes control the daily fluctuations or timing of the peak AOT_{500} at a particular location. In the case at Abracos Hill, the peak AOT_{500} simulated by the model is due to the transport of smoke from other burning sources. Of course over the entire continent, transport is a secondary consideration, and the temporal fluctuations in emissions dominate the spatial average AOT. In this study, the correlation between the model and AERONET AOT improves when emissions data sets with higher temporal resolutions are used in the model. These results suggest that variations in emissions may also play a role in the day-to-day fluctuations in AOT. Seeing that the model is generally a day off in simulating the correct timing of the peak AOT_{500} observed by AERONET (e.g., 16 and 18 September 2002 at Abracos Hill) suggests problems with the transport in the model on these days. However, the fact that the model does not simulate the high AOT_{500} between 20 and 25 September 2002 at Abracos Hill suggests problems in the smoke emissions. It is, however, difficult to draw conclusions concerning the model's transport and simulated AOT_{500} on a daily basis given the coarse resolution of the model. The coarse resolution makes it difficult to accurately simulate the spatial and temporal variability of the aerosol distributions because the spatial variations of the aerosol emissions and meteorological parameters become averaged out, washing out any details related to individual smoke events. Additionally, it is difficult generating daily and weekly emissions data sets given the large uncertainty

Table 4b. New Parameter Description for DMPS PSD

Mode	Number Fraction	Number Radius	Standard Deviation
1	0.086	0.006 μm	2.00
2	0.511	0.049 μm	1.74
3	0.403	0.103 μm	1.48

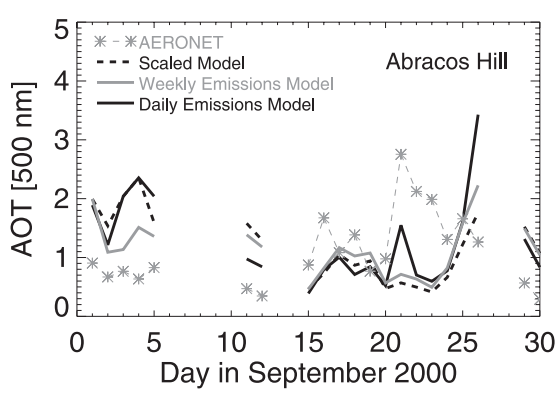

Figure 12. Daily mean AOT_{500} simulated by the scaled (black dashed line), daily emissions (black solid line), and weekly emissions (gray solid line) models, and retrieved by AERONET (asterisks/gray dashed line) at Abracos Hill during September 2002.

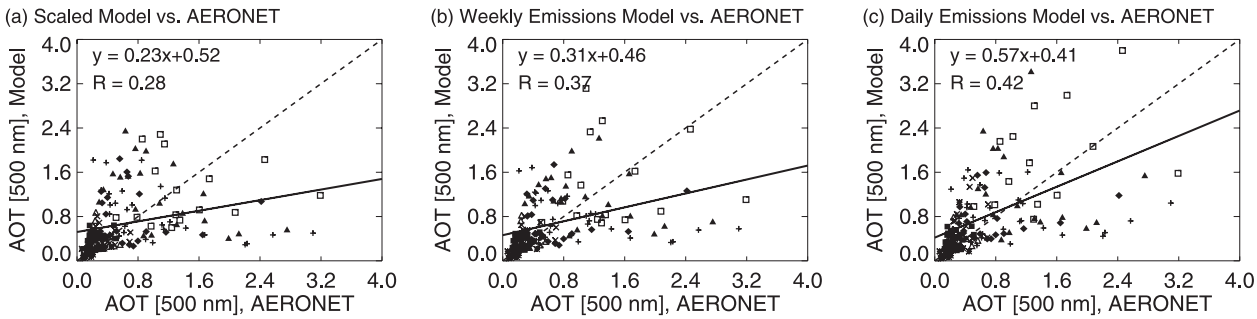

Figure 13. Scatterplots of daily mean AOT_{500} simulated by various models versus AERONET at selected study sites during September 2002. The dashed line represents the 1-to-1 line and the solid line represents the line of best fit. Each AERONET site is represented by a different symbol: Abracos Hill (solid triangle); Alta Floresta (open square); Balbina (solid square); Belterra (open triangle); CEILAP BA (star); Jaru Reserve (plus symbol); Rio Branco (solid diamond); Santa Cruz (cross symbol).

in the satellite information that is used to create these data sets. For instance, the satellite retrievals can be greatly impacted by cloud-contaminated pixels so the daily changes in burned area may be difficult for the satellites to retrieve, thereby making it difficult to generate a daily data set.

4.2. Sensitivity to Emitted Particle Size Distribution

[35] The sensitivity to different initial particle size distributions are investigated in this section. Instead of initializing the model with a particle size distribution retrieved by AERONET, a distribution measured by a Differential Mobility Particle Sizer (DMPS) is used as the emitted size distribution in the model and referred to as the "DMPS PSD" model (see gray solid line in Figure 1 and Tables 4a and 4b). Here, the initial particle size distribution only contains a fine mode distribution and is represented by lognormal size distributions using number concentrations, geometric median radii (r_N), and standard deviations (σ) measured by the DMPS instrument throughout the LBA–SMOCC campaign [*Rissler et al.*, 2006]. Briefly, this instrument was a ground-based instrument located at the Fazenda Nossa Senhora (FNS) Aparecida in the state of Rondonia in southwestern Amazonia, Brazil. This site was selected to sample particle size distributions during LBA–SMOCC since it can be representative of the region with extensive biomass burning during the dry season. The DMPS instrument measured particles with diameters between 3 and 850 nm in equal steps of logarithmic diameter from an inlet located about 5 m above the ground. The particle number size distributions were also measured at dry conditions (i.e., RH < 10%). Since this instrument only measured accumulation mode particles, the smoke emissions were adjusted to represent this size range. Thus, instead of using the GFEDv2 TPM emissions, the emissions data set for particulate matter ($PM_{2.5}$) provided by GFEDv2 is used in the DMPS PSD model. Again, in order to reproduce the observed AOT, the smoke source function needed to be scaled up by a factor of six.

[36] Since the DMPS PSD model only includes an accumulation mode, Table 5 shows the monthly mean optical properties of the accumulation mode fraction at selected locations. In comparisons between the DMPS PSD and scaled models, the monthly mean Ångström parameter (440/870 μm) of smoke-dominated days simulated by the DMPS PSD model decreased by less than 1% (Table 5). These results suggest that the DMPS model has slightly more larger-sized particles compared to the scaled model which uses a size distribution retrieved by AERONET. In general, there is about a 20% difference between the monthly mean AOT_{440} simulated by the DMPS PSD model and the scaled model and AERONET.

4.3. Sensitivity to Relative Humidity

[37] The sensitivity to relative humidity and subsequent hygroscopic growth is investigated in this section. Figure 14 shows the emitted particle size distribution, which represents the AERONET retrieved particle size distribution at Jaru Reserve on 20 September 2002, and its evolution as a function of relative humidity. Since the humidification parameterization only applies to the accumulation mode particles, the particle size distribution of this size range is shown in this figure. Here, the median radius of the accumulation mode increases from about 0.17 to 0.35 μm as the relative humidity increases from zero to 99%. To better understand how the particle size distribution changes with the humidification parameterization provided by *Rissler et al.* [2006], the Ångström parameter for the 440 and 870 nm wavelength pair at various levels of relative humidity is provided in the key of Figure 14. The same optics assumptions discussed in section 2.3 are used to compute the

Table 5. Monthly Mean Retrieved and Simulated Optical Properties of Smoke-Dominated Days at Selected Study Sites Over South America During September 2002[a]

	Abracos Hill, Brazil		Alta Floresta, Brazil		Jaru Reserve, Brazil		Rio Branco, Brazil	
	AOT_{440}	$\alpha_{440/870}$	AOT_{440}	$\alpha_{440/870}$	AOT_{440}	$\alpha_{440/870}$	AOT_{440}	$\alpha_{440/870}$
Number of days in mean	7	7	6	6	12	12	8	8
AERONET OBS.	1.25	1.96	1.46	1.93	1.28	1.98	0.87	1.94
Scaled	1.30	1.67	1.42	1.74	0.95	1.72	0.91	1.63
DMPS PSD	1.49	1.66	1.61	1.72	1.03	1.72	1.02	1.62

[a]These calculations only include the accumulation mode fraction.

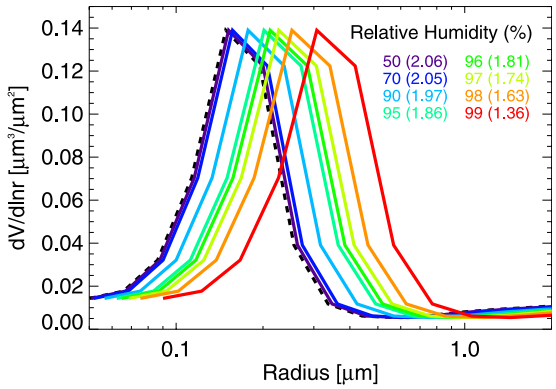

Figure 14. Particle size distribution as a function of relative humidity. This size distribution represents the AERONET retrieval at Jaru Reserve, Brazil on 20 September 2002. The black dashed line represents the initial particle size distribution at 0% (Ångström parameter = 2.02). The size distribution is swelled according to *Rissler et al.* [2006] parameterization using dry, midday average parameters. Also included in parentheses are the Ångström parameters of the particle distribution at the selected relative humidity values.

Ångström parameter. From 0% relative humidity to 50%, the Ångström parameter increases about 2%, whereas from 50% to 99% relative humidity the Ångström parameter decreases about 35%.

[38] To determine how sensitive the optical properties are to relative humidity and hygroscopic growth of the particles, a test was conducted where the relative humidity was assumed to be zero everywhere in the model domain. This test is referred to as the "no hygroscopic growth" model (Table 4a). When the relative humidity is assumed to be zero, the monthly mean AOT_{500} of smoke-dominated days decreases by about 15% and Ångström parameter increases by about 10% (see Table 2). Even though the monthly mean Ångström parameter simulated by the no hygroscopic growth model is more comparable to the AERONET retrievals than the scaled model at some locations, the daily Ångström parameter simulated by the no hygroscopic growth model is not as variable as AERONET (Figure 15). Here the daily mean Ångström parameter simulated by the no hygroscopic growth model varies from about 1.5 to 1.9, where the AERONET ranges from about 0.5 to 2.2. The daily mean Ångström parameter simulated by the scaled model ranges from about 0.97 to 1.94. Additionally, the smoke aerosols become about 10% more absorbing when the relative humidity is assumed to be zero (Figure 8 and Table 2). The effects of relative humidity are more significant over South America than the results found over southern Africa in the work of *Matichuk et al.* [2007]. These results are expected, since the monthly mean relative humidity reported by MATCH over South America is greater than 70%, whereas over southern Africa the relative humidity is less than 45%.

[39] Since one could question the impact of humidity on optical properties from the model, data from South America were analyzed and also show the single scattering albedo varying with humidity. Figure 16 compares the monthly mean SSA_{440} retrieved by AERONET over South America and the relative humidity averaged between the surface and 3 km provided by MATCH. The results show a strong correlation where SSA increases with increasing relative humidity (Figure 16). These results are expected knowing that water is less absorbing than smoke. Therefore, an increase in water content on the aerosol will increase the SSA.

4.4. Sensitivity to Wet Removal

[40] A study by *Koren et al.* [2004] used MODIS-Aqua data to suggest that smoke from fires reduced the area covered by clouds over the Amazon Basin during the dry season of 2002. In the afternoons, cumulus clouds were commonly found to develop uniformly over the Amazon forest region when the overlying air was not filled with high concentrations of smoke. However, as the smoke column concentration increased, *Koren et al.* [2004] found that the cloud cover fraction decreased continuously as a function of smoke AOT. In addition, the competition for water vapor by the extremely high concentrations of particles was suggested to inhibit the clouds from having large droplets, thereby suppressing coalescence and precipitation.

[41] Since most wet removal parameterizations used in climate models do not include the suppression of cloud formation and precipitation due to smoke aerosols, this section suggests the potential errors that may arise in the

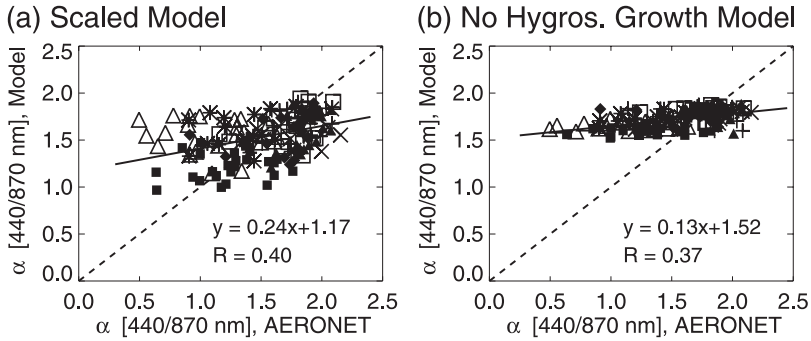

Figure 15. Scatterplots of daily mean Ångström parameter (440/870 nm) simulated by various models versus AERONET at selected study sites during September 2002. The dashed line represents the 1-to-1 line and the solid line represents the line of best fit. Each AERONET site is represented by a different symbol: Abracos Hill (solid triangle); Alta Floresta (open square); Balbina (filled square); Belterra (open triangle); CEILAP BA (star); Jaru Reserve (plus symbol); Rio Branco (solid diamond); Santa Cruz (cross symbol).

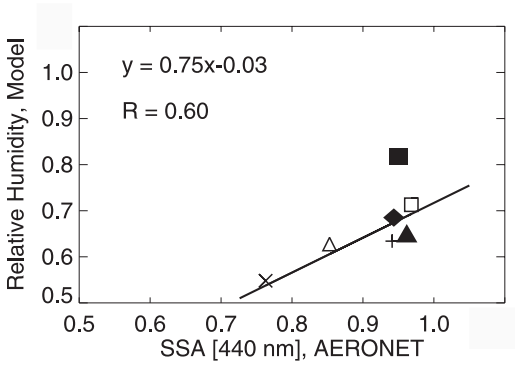

Figure 16. Monthly mean SSA_{440} retrieved by AERONET and relative humidity provided by MATCH averaged between the surface and 3 km at selected study sites during September 2002. The black solid line represents the line of best fit. Each AERONET site is represented by a different symbol: Abracos Hill (solid triangle); Alta Floresta (open square); Balbina (solid square); Belterra (open triangle); CEILAP BA (star); Jaru Reserve (plus symbol); Rio Branco (solid diamond); Santa Cruz (cross symbol).

simulated optical properties from not including the impacts of smoke aerosols properly. Briefly, the wet removal parameterization used in the model follows *Barth et al.* [2000] where the scavenging is treated as a first-order loss process. The wet removal of smoke aerosols is independent of particle size and can be affected by cumulus precipitation or stratiform precipitation and evaporation. The details of the wet removal scheme used in CARMA are discussed by *Colarco et al.* [2003a, 2003b].

[42] To determine the sensitivity in the simulated optical properties due to the wet removal of smoke aerosols, three additional test simulations are conducted in this section. In one test, a simulation where the wet removal of smoke aerosols is turned off is conducted and referred to as the "no wet removal" model (Tables 2 and 4a). In the other two tests, simulations are conducted to investigate the feedback suggested by *Koren et al.* [2004]. In these tests, the cloud fraction (CF) used in the model's wet removal routine is defined by using the functions reported by *Koren et al.* [2004, Figure 3]. On the basis of the east and west CF data presented in Figure 3 from *Koren et al.* [2004], the estimated slope of the CF as a function of AOT is −0.35. To make the function from *Koren et al.* [2004] consistent with our model, the CF is assumed to be the CF_{MATCH} determined by MATCH when the AOT is zero. In this case, the new CF in the model is defined as

$$CF = -0.35AOT + CF_{\mathrm{MATCH}} \quad (1)$$

where AOT is the column AOT at 550 nm and CF_{MATCH} is the cloud fraction provided by MATCH at the current time step. Since this feedback by *Koren et al.* [2004] was found in observations of cumulus clouds, a test is conducted where the model's cloud fraction is modified only in the convective scavenging calculations, and referred to as the "feedback 1" model (Tables 2 and 4a). However, if the stratus clouds form in the boundary layer, where most of the smoke aerosols are trapped, stratus clouds may also be impacted by the smoke aerosols. Therefore, another simulation is conducted where the cloud fraction is estimated using the function defined by *Koren et al.* [2004] in the convective scavenging calculations and in the stratiform scavenging calculations that occur in the boundary layer. This simulation is referred to as the "feedback 2" model (Tables 2 and 4a).

[43] Figure 17 presents scatterplots of the monthly mean AOT_{550} simulated by these models versus observations over continental South America during September 2002. When wet removal of the smoke aerosols is turned off in the model, the simulated monthly mean AOT_{550} over South America essentially increases by about 35% (i.e., compare the regression line in Figure 17a with Figure 4a and Figure 17d with Figure 4b). However at the selected AERONET sites, the simulated AOT_{500} increases by up to 90% when the smoke aerosols are not removed by wet scavenging (see scaled and no wet removal model in Table 2). When the feedback function is applied to convective and stratiform scavenging, the simulated AOT increases by up to 35% relative to the scaled model (i.e., compare regression lines in Figures 17b and 17c with Figure 4a and Figures 17e and 17f with Figure 4b and Table 2). When the uncertainty in the smoke source function is considered by scaling the smoke emissions up by a factor of three (instead of the factor of six used in the "scaled" model) and the same three tests are conducted, the monthly mean simulated AOT is within 50% of the observations (results not shown). In this case, the average slope of the regression lines in the model comparisons against MODIS and MISR are about 0.70, 0.53, and 0.57 for the no wet removal, feedback 1, and feedback 2 tests, respectively.

[44] These results suggest that clouds and precipitation are important removal mechanisms in the model. To understand the cloud and precipitation parameters used in the model, these parameters are compared to observations. Since MATCH determines the total cloud fraction in a grid cell at an individual layer, the monthly mean cloud fraction averaged over the boundary layer from the model is compared to the monthly mean AOT_{500} retrieved by AERONET (Figure 18). Similar to *Koren et al.* [2004], the cloud fraction simulated by MATCH is strongly correlated to the AOT_{500} retrieved by AERONET. However, the slope of the line of best fit is slightly less than that found by *Koren et al.* [2004]. These results suggest that the model implicitly includes the feedback in the cloud fraction, probably because the smoke stabilizes the boundary layer which is identified in the NCEP meteorological data. In addition to cloud fraction comparisons, the precipitation rate simulated by MATCH is compared to the Global Precipitation Climatology Project (GPCP) [*Huffman et al.*, 2001]. The monthly mean precipitation rate simulated by MATCH over South America during September 2002 is about 20% higher than the GPCP (results not shown; regression line is $y = 0.82\times + 0.00$; $R = 0.67$), suggesting that the precipitation provided by MATCH may be too high and may possibly be removing too many smoke aerosols.

[45] Overall, by not treating the impacts smoke aerosols have on cloud formation and subsequent wet removal in the model, the simulated AOT can potentially be overestimated and to some extent explain the large scaling factor applied to the smoke emissions. It is difficult to determine how much of the scaling factor is due to the overly aggressive wet removal seeing that the NCEP meteorological data may

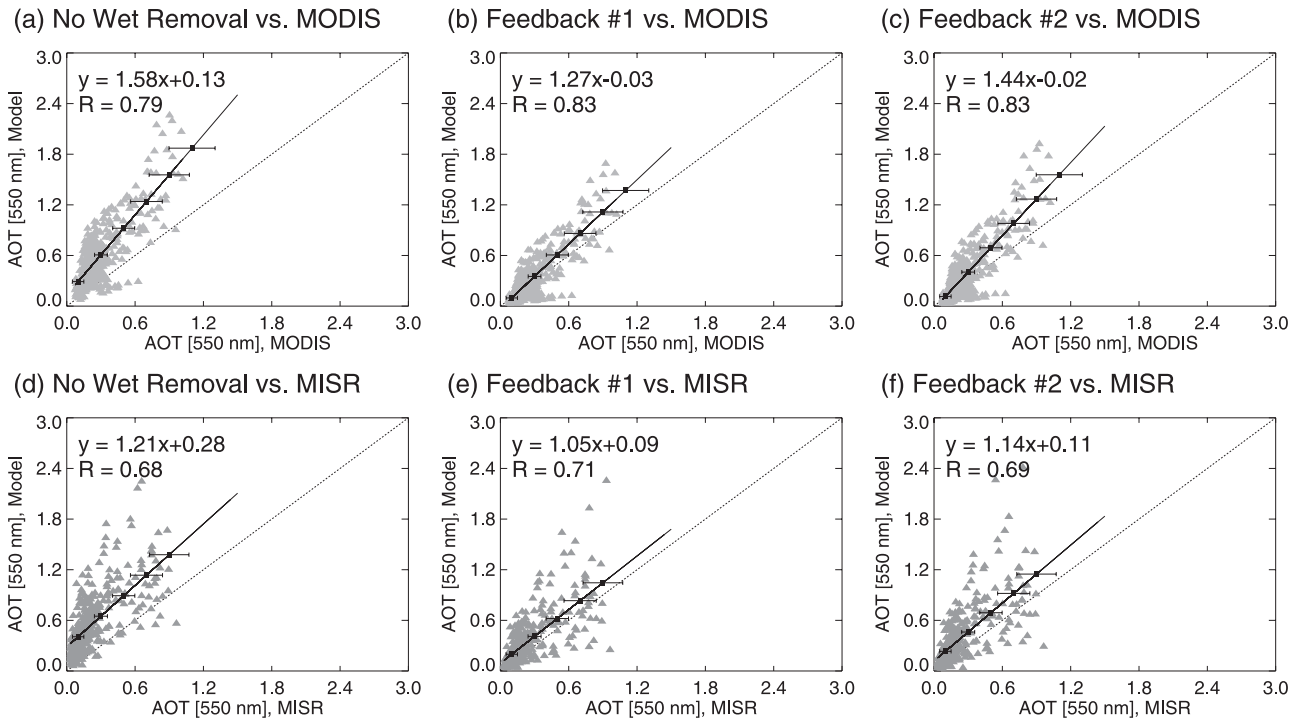

Figure 17. Scatterplots of monthly mean AOT_{500} simulated various models versus satellite observations over South America during September 2002. The dashed line represents the 1-to-1 line and the solid line represents the line of best fit. For clarity, the uncertainty in the satellite retrievals is grouped into intervals of 0.20. The error bars in these figures represent the mean uncertainty in the satellite data at each interval. (a) No wet removal model versus MODIS; (b) feedback 1 model versus MODIS; (c) feedback 2 model versus MODIS; (d) no wet removal model versus MISR; (e) feedback 1 model versus MISR; (f) feedback 2 model versus MISR.

be implicitly including this feedback suggested by *Koren et al.* [2004]. However, even without any rainout, a scaling factor of about two is required to obtain the observed AOT. Since clouds are not physically treated in this model, the development of a wet removal parameterization that considers more realistic interactions between smoke and clouds is a subject of future research.

5. Similarities Between African Savanna and South American Forest Smoke Simulations

[46] Comparisons between African savanna and South American forest smoke simulations suggest that these two smoke sources are very similar. In this section, two additional sensitivity tests are conducted. In the first test, the same particle size distribution and optical property assumptions used in the work of *Matichuk et al.* [2007] to simulate African savanna fires are used to simulate smoke plumes over South America. This test is referred to as "African conditions" (Tables 2 and 4a). Here, a particle size distribution representative of an almucantar scan retrieved by AERONET at Ndola, Zambia on 16 September 2000 and the mean refractive index of smoke-dominated days as retrieved by AERONET at 440 nm at Ndola during September 2000 ($1.51-0.024i$) are applied in this test. The humidification parameterization provided by *Magi and Hobbs* [2003] and used by *Matichuk et al.* [2007] is not incorporated in this test since it does not work well with a model that evolves a particle size distribution. Instead, the volume weighting approach discussed above and the humidification parameterization provided by *Rissler et al.* [2006] is used. Using the same smoke emissions derived from GFEDv2 that are used in the scaled model, the monthly mean AOT_{500} of smoke-dominated days simulated by the African conditions model is about 10% lower and the aerosols are slightly more absorbing than the scaled

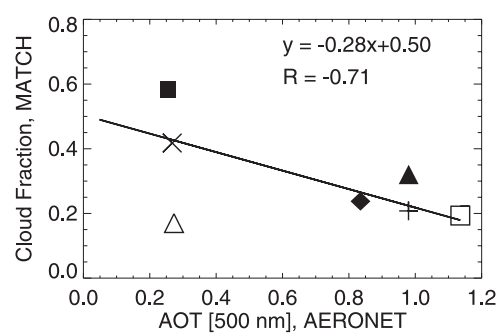

Figure 18. Monthly mean AOT_{500} retrieved by AERONET and total cloud fraction average through the boundary layer simulated by MATCH at selected study sites during September 2002. The black solid line represents the line of best fit. Each AERONET site is represented by a different symbol: Abracos Hill (solid triangle); Alta Floresta (open square); Balbina (solid square); Belterra (open triangle); CEILAP BA (star); Jaru Reserve (plus symbol); Rio Branco (solid diamond); Santa Cruz (cross symbol).

model (Table 2). The monthly mean Ångström parameter simulated by the African conditions model is slightly lower than the scaled model suggesting that this model has more larger-sized particles. Since the volume of the coarse mode in the Ndola particle size distribution is higher than the Jaru Reserve size distribution (see black dashed line and black solid line, respectively, in Figure 1), the AOT simulated by the African conditions model is lower than the scaled model. In this case, mass in the accumulation mode is more optically efficient, than mass in the coarse mode.

[47] To further investigate how the African particle size distribution functions over South America, an additional test is conducted. For this test, the African particle size distribution and South American refractive index, volume weighting approach discussed above and humidification parameterization provided by *Rissler et al.* [2006] are used to simulate smoke plumes over South America. This case is referred to as the "African PSD" model (Tables 2 and 4a). Compared to the scaled model, the monthly mean Ångström parameter simulated by the African PSD model is slightly lower. These results are expected since the Ndola particle size distribution (see black dashed line in Figure 1) has a larger coarse mode volume than the Jaru Reserve distribution (see black solid line in Figure 1). In comparisons of the spectral dependence of SSA, the results of the African PSD model are within the uncertainty of the AERONET retrievals (see gray solid line in Figure 8).

[48] Overall, since the particle size distributions used to simulate African and South American biomass burning aerosols are similar, these results suggest that the humidification parameterization is an important factor in simulating the differences between the optical properties of African and South American smoke plumes. The different relative humidity levels between each region can explain the differences found between the single scattering albedo of African smoke and South American smoke. Therefore in this study, there is no evidence that compositional differences between the aerosols emitted from these regions, nor the deposition of aerosol mass from the gas phase, is of importance. This suggests that any compositional differences do not impact the particle size, or optical properties, and that any gas to particle conversion occurs on spatial scales that are smaller than the model's grid resolution.

6. Uncertainties in the Simulation of Smoke Aerosols

[49] While satellite observations and in situ measurements have been utilized in the detection and quantification of aerosols, modeling efforts are essential for providing future predictions of the aerosol effects on climate. Much progress has been made in the modeling aerosols; however, modelers are consistently challenged by the temporal and spatial variability in the aerosol distributions, aerosol composition, and aerosol shape. In this study, the simulated smoke source strength, the time of injection during the day and month, transport, initial particle size distribution, and aging and removal processes (i.e., coagulation, humidification, and dry and wet removal) all significantly affect the amount and distribution of the aerosol mass. Any uncertainty in these components will ultimately affect the model results and optical properties of the smoke aerosols.

[50] As mentioned previously, in order to reproduce the observed AOT over South America, the smoke emissions used in the model need to be scaled up by about a factor of six. This scaling factor is not well defined since there is evidence of a positive feedback between wet removal and smoke, which is not included in the current model's wet removal scheme. The contribution from other aerosol sources (e.g., dust, sea salt, anthropogenic and biogenic sources) that may exist in this region may also affect the magnitude of the scaling factor. In this case, other aerosol sources could potentially lower the scaling factor applied to the smoke emissions for the model to be comparable to the observations. Nevertheless, the smoke emission rate is one important factor that produces large errors in the simulated AOT.

[51] Modeling errors may also influence the simulated AOT. As shown above in section 4, the incorrect representation of wet scavenging in regions dominated by biomass burning may generate errors in the simulated AOT. The uncertainties in the humidification of the smoke aerosols may also impact the simulated AOT. In addition, the contribution of other aerosol species will impact all of the simulated optical properties. In this case, adding other aerosol sources may impact the particle size distribution, humidification, and absorption properties of the aerosols.

7. Conclusions

[52] In this study, a set of measurement-based initial conditions have been developed to specify the aerosol emissions, injection altitude, particle size distribution, and optical properties in a global climate model to simulate smoke plumes originating over South America during the LBA–SMOCC campaign. In general, the model compares fairly well to satellite and ground-based observations of AOT, Ångström parameters, and single scattering albedo on a monthly basis. The monthly mean spatial distribution of the aerosol loading over South America also compares well to satellites, suggesting that the transport processes in the model are adequate over this region. Similar to previous work over southern Africa, this study also finds that the day-to-day variations in AOT at a given location are controlled by transport processes. However, the correlations between the daily mean AOT simulated by the model and AERONET retrievals are found to improve when emissions data sets with finer temporal resolutions are used in the model. The average AOT over South America of course is controlled by emissions, rather than transport. In comparisons of vertical extinction profiles, the model compares well to MPLNET, suggesting that the vertical transport in the model is adequate at this location. Since the SSA observed by AERONET and simulated by the model decreases with increasing wavelength and the simulated spectral dependence uses a wavelength independent refractive index suggest that the absorbing aerosols in this region are relatively small black carbon (BC) particles. Comparisons of the spectral dependence and magnitude of SSA also suggest that relative humidity and subsequent hygroscopic growth of the smoke aerosol plays an important role in reproducing the observed SSA and variability in Ångström

parameter. The results from this study further suggest that the emissions provided by GFEDv2 are too low over this region. It is difficult to determine the factor by which the emissions are low since the simulated AOT of smoke aerosols is significantly impacted by the wet removal parameterization in the model. Other studies have suggested that the smoke will suppress rainfall, but this feedback is not explicitly included in our model. In attempts to incorporate this feedback and adjust the cloud fraction in the model according to *Koren et al.* [2004], the simulated AOT is found to increase by up to 90% at individual locations and about 35% regionally. Therefore, incorporating this feedback in the model could account for some of the scaling used in the smoke emissions. However, the atmospheric stability over South America may be implicitly present in the NCEP data so that the feedback is included in models running from analyzed data. Since this study only includes aerosols from biomass burning, other sources (e.g., sea salt, dust, and biogenic and anthropogenic sources) that may exist over this region may also explain some of the scaling used in the smoke emissions. We also found similarities between African and South American biomass burning aerosols and conclude that the same size distributions and aerosol optical properties can be used to simulate smoke aerosols in either location. However, relative humidity is very different between Africa and South America. We find that significant differences in the observed SSA of the smoke in the two regions are due not to source properties but to relative humidity. In particular, any differences in the chemical compositions between South American and southern African smoke do not seem to be significant to the optical properties calculated in this study. Additionally, there is no evidence that gas to particle conversion is of significance, though it may occur over smaller spatial scales than what the model can resolve. Data from South America are provided to confirm the dependence of SSA on humidity. Overall, this work is a step toward improved quantification of smoke aerosol optical properties for use in calculating the direct effects of these aerosols on climate and provides a strategy for the incorporation of particle size distributions into microphysical models.

[53] **Acknowledgments.** This work was supported by NSF-ATM0435713 and NIP/03-0000-0043. Rebecca Matichuk was partially supported by the NASA Goddard GSRP program. We would like to thank the following people and groups for kindly providing data and assisting us with the satellite and ground-based data used in our study: AERONET and MPLNET staff (PI: B. Holben) at the NASA Earth Observatory System and Radiation Sciences Program for establishing and maintaining the measurements used in this investigation, MISR and MODIS teams, G. van der Werf (GFED data), and A. daSilva (QFED data). We would also like to thank the reviewers for their time, thoughtful comments, and suggestions.

References

Ackerman, A., O. Toon, and P. Hobbs (1995), A model for particle microphysics, turbulent mixing, and radiative-transfer in the stratocumulus-topped marine boundary-layer and comparisons with measurements, *J. Atmos. Sci.*, *52*(8), 1204–1236.

Andreae, M. O., and P. Merlet (2001), Emission of trace gases and aerosols from biomass burning, *Global Biogeochem. Cycles*, *15*(4), 955–966.

Andreae, M. O., D. Rosenfeld, P. Artaxo, A. Coasta, G. Frank, K. Longo, and M. Silvia-Dias (2004), Smoking rain clouds over the Amazon, *Science*, *303*, 1337–1342.

Barth, M. C., P. J. Rasch, J. T. Kiehl, C. M. Benkovitz, and S. E. Schwartz (2000), Sulfur chemistry in the National Center for Atmospheric Research Community Climate Model: Description, evaluation, features, and sensitivity to aqueous chemistry, *J. Geophys. Res.*, *105*(D1), 1387–1416.

Bergstrom, R., P. Russell, and P. Hignett (2002), Wavelength dependence of the absorption of black carbon particles: Predictions and results from the TARFOX experiment and implications for the aerosol single scattering albedo, *J. Atmos. Sci.*, *59*(59), 567–577.

Chand, D., P. Guyon, P. Artaxo, O. Schmid, G. Frank, L. Rizzo, O. Mayol-Bracero, L. Gatti, and M. Andreae (2006), Optical and physical properties of aerosols in the boundary layer and free troposphere over the Amazon Basin during the biomass burning season, *Atmos. Chem. Phys.*, *6*, 2911–2925.

Colarco, P. R., O. B. Toon, O. Torres, and P. J. Rasch (2002), Determining the UV imaginary index of refraction of Saharan dust particles from Total Ozone Mapping Spectrometer data using a three-dimensional model of dust transport, *J. Geophys. Res.*, *107*(D16), 4289, doi:10.1029/2001JD000903.

Colarco, P. R., O. B. Toon, and B. N. Holben (2003a), Saharan dust transport to the Caribbean during PRIDE: 1. Influence of dust sources and removal mechanisms on the timing and magnitude of downwind aerosol optical depth events from simulations of in situ and remote sensing observations, *J. Geophys. Res.*, *108*(D19), 8589, doi:10.1029/2002JD002658.

Colarco, P. R., et al. (2003b), Saharan dust transport to the Caribbean during PRIDE: 2. Transport, vertical profiles, and deposition in simulations of in situ and remote sensing observations, *J. Geophys. Res.*, *108*(D19), 8590, doi:10.1029/2002JD002659.

Colarco, P. R., M. R. Schoeberl, B. G. Doddridge, L. T. Marufu, O. Torres, and E. J. Welton (2004), Transport of smoke from Canadian forest fires to the surface near Washington, D.C.: Injection height, entrainment, and optical properties, *J. Geophys. Res.*, *109*, D06203, doi:10.1029/2003JD004248.

Crutzen, O. J., and M. O. Andreae (1990), Biomass burning in the tropics – Impact on atmospheric chemistry and biogeochemical cycles, *Science*, *250*, 669–1678.

Deeter, M. N., et al. (2003), Operational carbon monoxide retrieval algorithm and selected results for the MOPITT instrument, *J. Geophys. Res.*, *108*(D14), 4399, doi:10.1029/2002JD003186.

Diner, D. J., et al. (1998), Multiangle imaging spectrometer (MISR) instrument description and experiment overview, *IEEE Trans. Geosci. Remote Sens.*, *36*, 1072–1087.

Dubovik, O., and M. D. King (2000), A flexible inversion algorithm for retrieval of aerosol optical properties from Sun and sky radiance measurements, *J. Geophys. Res.*, *105*(D16), 20,673–20,696.

Eck, T. F., B. N. Holben, J. S. Reid, O. Dubovik, A. Smirnov, N. T. O'Neill, I. Slutsker, and S. Kinne (1999), Wavelength dependence of the optical depth of biomass burning, urban, and desert dust aerosols, *J. Geophys. Res.*, *104*(D24), 31,333–31,350.

Giglio, L., J. D. Kendall, and R. Mack (2003a), A multi-year active fire data set for the tropics derived from the TRMM VIRS, *Int. J. Remote Sens.*, *24*, 4505–4525.

Giglio, L., J. J. Descloitres, C. O. Justice, and Y. J. Kaufman (2003b), An enhanced contextual fire detection algorithm for MODIS, *Remote Sens. Environ.*, *87*(2–3), 273–282.

Giglio, L., G. R. van der Werf, J. T. Randerson, G. J. Collatz, and P. S. Kasibhatla (2006), Global estimation of burned area using MODIS active fire observations, *Atmos. Chem. Phys.*, *6*, 957–974.

Hao, W. M., M. H. Liu, and P. J. Crutzen (1990), Estimates of annual and regional releases of CO_2 and their trace gases to the atmosphere from fires in the tropics, based on the FAO statistics for the period 1975–1980, in *Fire in the Tropical Biota: Ecosystem Processes and Global Challenges*, *Ecol. Stud.*, vol. 84, edited by J. G. Goldammer, pp. 440–462, Springer, New York.

Holben, B. N., et al. (1998), AERONET-A federated instrument network and data archive for aerosol characterization, *Remote Sens. Environ.*, *66*(1), 1–16.

Huffman, G. J., R. F. Adler, and M. M. Morrissey (2001), Global precipitation at one-degree daily resolution from multisatellite observations, *J. Hydrometeorol.*, *2*(1), 36–50.

Intergovernmental Panel on Climate Change (2001), *Climate Change 2001: The Scientific Basis: Contribution of Working Group I to the Third Assessment Report of the Intergovernmental Panel on Climate Change*, edited by J. T. Houghton et al., 881 pp., Cambridge Univ. Press, New York.

Kalnay, E., et al. (1996), The NCEP/NCAR 40-year reanalysis project, *Bull. Am. Meteorol. Soc.*, *77*, 437–471.

Kaufman, Y. J., D. Tanré, L. A. Remer, E. F. Vermote, A. Chu, and B. N. Holben (1997), Operational remote sensing of tropospheric aerosol over land from EOS moderate resolution imaging spectroradiometer, *J. Geophys. Res.*, *102*(D14), 17,051–17,068.

Koren, I., Y. Kaufman, L. Remer, and J. Martins (2004), Measurement of the effect of Amazon smoke on inhibition of cloud formation, *Science*, *303*, 1342–1345.

Lavoué, D., C. Liousse, H. Cachier, B. Stocks, and J. Goldammer (2000), Modeling of carbonaceous particles emitted by boreal and temperate wildfires at northern latitudes, *J. Geophys. Res.*, *105*(D22), 26,871–26,890.

Lin, S. J., and R. B. Rood (1996), Multidimensional flux-form semi-Lagrangian transport schemes, *Mon. Weather Rev.*, *124*, 2046–2070.

Magi, B. I., and P. V. Hobbs (2003), Effects of humidity on aerosols in southern Africa during the biomass burning season, *J. Geophys. Res.*, *108*(D13), 8495, doi:10.1029/2002JD002144.

Martonchik, J., D. Diner, R. Kahn, T. Ackerman, M. Verstraete, B. Pinty, and H. Gordon (1998), Techniques for the retrieval of aerosol properties over land and ocean using Multiangle imaging, *IEEE Trans. Geosci. Remote Sens.*, *36*, 1212–1227.

Matichuk, R., P. Colarco, J. Smith, and O. Toon (2007), Modeling the transport and optical properties of smoke aerosols from African savanna fires during SAFARI 2000, *J. Geophys. Res.*, *112*, D08203, doi:10.1029/2006JD007528.

Myhre, G., T. K. Berntsen, J. M. Haywood, J. K. Sundet, B. N. Holben, M. Johnsrud, and F. Stordal (2003), Modeling the solar radiative impact of aerosols from biomass burning during the Southern African Regional Science Initiative (SAFARI-2000) experiment, *J. Geophys. Res.*, *108*(D13), 8501, doi:10.1029/2002JD002313.

Prins, E., J. Feltz, W. Menzel, and D. Ward (1998), An overview of GOES-8 diurnal fire and smoke results for SCAR-B and 1995 fire season in South America, *J. Geophys. Res.*, *103*(D24), 31,821–31,835.

Pruppacher, H. R., and J. D. Klett (1997), *Microphysics of Clouds and Precipitation*, Springer, New York.

Rasch, P. J., N. M. Mahowald, and B. E. Eaton (1997), Representations of transport, convection, and the hydrologic cycle in chemical transport models: Implications for the modeling of short-lived and soluble species, *J. Geophys. Res.*, *102*(D23), 28,127–28,138.

Reid, J. S., P. V. Hobbs, R. J. Ferek, D. R. Blake, J. V. Martins, M. R. Dunlap, and C. Liousse (1998), Physical, chemical, and optical properties of regional hazes dominated by smoke in Brazil, *J. Geophys. Res.*, *103*(D24), 32,059–32,080.

Reid, J. S., R. Koppmann, T. Eck, and D. Eleuterio (2004), A review of biomass burning emissions, part II: Intensive physical properties of biomass burning particles, *Atmos. Chem. Phys. Disc.*, *4*, 5135–5200.

Rissler, J., A. Vestin, E. Swietlicki, G. Fisch, J. Zhou, P. Artaxo, and M. Andreae (2006), Size distribution and hygroscopic properties of aerosol particles from dry-season biomass burning in Amazonia, *Atmos. Chem. Phys.*, *6*, 471–491.

Smirnov, A., B. N. Holben, T. F. Eck, O. Dubovik, and I. Slutsker (2000), Cloud screening and quality control algorithms for the AERONET database, *Remote Sens. Environ.*, *73*, 337–349.

Spinhirne, J. D., J. Rall, and V. S. Scott (1995), Compact eye safe lidar systems, *Rev. Laser Eng.*, *23*, 112–118.

Tanré, D., Y. J. Kaufman, M. Herman, and S. Mattoo (1997), Remote sensing of aerosol properties over oceans using the MODIS/EOS spectral radiances, *J. Geophys. Res.*, *102*(D14), 11,201–11,218.

Toon, O. B., R. Turco, D. Westphal, R. Malone, and M. Liu (1988), A multidimensional model for aerosols: Description of computational analogs, *J. Atmos. Sci.*, *45*(15), 2123–2144.

Van der Werf, G. R., J. T. Randerson, J. Collatz, and L. Giglios (2003), Carbon emissions from fires in tropical and subtropical ecosystems, *Global Change Biol.*, *9*(4), 547–562.

Van der Werf, G. R., J. T. Randerson, L. Giglio, G. J. Collatz, and P. S. Kasibhatla (2006), Interannual variability in global biomass burning emission from 1997 to 2004, *Atmos. Chem. Phys.*, *6*, 3423–3441.

Warner, J., and S. Twomey (1967), The production of cloud nuclei by cane fires and the effect on cloud drop concentrations, *J. Atmos. Sci.*, *24*, 704–706.

Westphal, D. L., and O. B. Toon (1991), Simulations of microphysical, radiative, and dynamical processes in a continental-scale forest fire smoke plume, *J. Geophys. Res.*, *96*(D12), 22,379–22,400.

Winker, D. M., J. Pelon, and M. P. McCormick (2002), The CALIPSO mission: Spaceborne lidar for observation of aerosols and clouds, *Proc. SPIE Int. Soc. Opt. Eng.*, *4893*, 1–11.

Wiscombe, W. (1979), Mie scattering calculations: Advances in technique and fast, vector-speed computer codes, *Tech. Note TN-140+STR*, Natl. Cent. for Atmos. Res., Boulder, Colo.

Zhang, L., S. Gong, J. Padro, and L. Barrie (2001), A size-segregated particle dry deposition scheme for an atmospheric aerosol module, *Atmos. Environ.*, *35*(3), 549–560.

P. R. Colarco, NASA Goddard Space Flight Center, Code 613.3, Greenbelt, MD 20771, USA.

R. I. Matichuk, Earth System Research Laboratory, NOAA, Boulder, CO 80305, USA. (rebecca.matichuk@noaa.gov)

J. A. Smith and O. B. Toon, Laboratory for Atmospheric and Space Physics, Department of Atmospheric and Oceanic Sciences, University of Colorado, Boulder, CO 80309, USA.